THE STRUCTURAL AND CHEMICAL ANALYZER (SCA) SYSTEM FOR THE ANALYSIS OF DEPOSITED ATMOSPHERIC PARTICLES AND DEGRADATION COMPOUNDS PRESENT ON THE SURFACE OF OUTDOORS WEATHERING STEEL OBJECTS

J. Aramendia*, L. Gomez-Nubla, K. Castro, and J.M. Madariaga.

*Department of Analytical Chemistry, University of the Basque Country UPV/EHU , P.O.Box 644, E-48080 Bilbao, Spain, +34 946018297, *julene.aramendia@ehu.es*

ABSTRACT

The weathering steel is a high strength low alloy special kind of steel which is theoretically resistant to the atmospheric corrosion. This feature makes this material very suitable for employing it in works exposed outdoors. However, it is also known that the presence of some pollutants in high concentrations can degrade the structure reducing its characteristic protective ability and its lifetime. Moreover, it has been reported that the presence of some silicate matter in the steel surface, induces the retard of the transformation of the active form of iron oxy-hydroxide lepidocrocite into the passive form goethite and therefore, the passivation rate of the rust layer, being this passivation crucial for the protective function of this layer. In the present work, several weathering steel structures exposed to the urban atmosphere were analyzed by means of SCA (Structural and Chemical Analyzer), an spectroscopic system that combines micro-Raman and SEM/EDX microscopy measurements in the same spot, in order to detect the deposited atmospheric material and to characterize it. Several kinds of silicates and aluminosilicates containing particles were identified on the steel surface of the analysed works. In addition, other atmospheric particles such as calcite, charcoal and chromium rich particles were detected together with several compounds coming from the reaction of the steel and the deposited particles with the acid gases of the atmosphere.

KEYWORDS: SCA, weathering steel, atmospheric particles, urban atmosphere, marine atmosphere.

1. INTRODUCTION

Even though weathering steel was developed for its use in architecture and sculpture, sometimes, due to the exposition of this material to certain atmospheric conditions, it is possible to observe uncontrolled corrosion probably due to an unusual development of the protective patina. This patina is composed by a mixture of iron oxides and its composition changes from the most reactive lepidocrocite to the most stable goethite with the exposure time. One of the most famous weathering steel washouts is the former Omni Coliseum (Atlanta, Georgia, USA). It never stopped rusting, and eventually large holes appeared in the structure. This was the major factor in the decision to demolish it just 25 years after its construction [1]. Besides, the use of weathering steel outdoors presents further problems. During the initial weathering

process, considerable quantities of dissolved iron (II) are washed off, which can cause staining of adjacent surfaces, especially in porous materials such as concrete and masonry, because the colorless Fe^{2+} cation is oxidized to the yellow-orange Fe(III) oxy-hydroxides. An example of this fact is the U.S. Steel Tower in Pittsburgh, Pennsylvania (USA). The initial weathering of the material resulted in a coloration of the surrounding city sidewalks as well as other nearby buildings [2].

The main factor that could induce these problems is the damage caused by pollutants and atmospheric particles affecting to the durability of the material. The chemical composition of the atmosphere is of special significance for the thermodynamics and kinetics of the corrosion process. For instance, it is known that certain high concentrations of acid gases such as SO_2 together with a high humidity modify the natural or normal weathering process of steel, while high concentration of these acid gases could lead to serious problems in the development of the protective rust layer [3]. Actually, SO_2 is considered the worst factor affecting to the corrosion process. Together with SO_2, other gaseous pollutants such as NO_x, CO_2 and O_3 are reportedly the most significant species involved in atmospheric corrosion [4]. The action of these gases causes the increase of the corrosion rate in metals through a mechanism known as deposition. The most harmful mechanism is the so-called wet deposition in which the decay pattern starts with the reaction of the pollutants cited above with rain water or humidity, giving rise to their respective acid aerosols (H_2CO_3, H_2SO_4 and HNO_3) [5]. This results on the formation of soluble salts such as sulphates and nitrates after the acid attack of the aerosols against the metallic material and/or against the atmospheric particles deposited on the metallic surface. The presence of salts and gases dissolved in a moisture film over the metal surface can generate the dissolution of the metal, accelerating the corrosion process.

These degradation mechanisms have been widely studied and nowadays they are well known. However, the corrosion process depends not only on atmospheric acid gases but also on the composition of the electrolyte that wets the metal surface. The different compounds present in the atmosphere can be dissolved in this electrolyte triggering several consequences on the rate of corrosion [6, 7]. These compounds, mostly atmospheric particles, could be very different depending on the atmosphere where the structure is exposed to. Unfortunately, the effect of some of them has not been deeply studied.

Albeit there are some atmospheric particles and airborne whose effects in the weathering steel are well known. For instance, an important factor that accelerates the corrosion process in weathering steel is the marine airborne which is mainly composed by sodium chloride (NaCl). The influence of chloride ions may be severe, especially in environments near to the coast. It

has been noticed that weathering steel does not form a well protective patina in the presence of chlorides [8, 9]. This is due in part to the hygroscopic characteristics of the salt that keeps the steel moist for longer periods of time, preventing the occurrence of dry conditions necessary for the patina formation. The other factor is that the presence of chloride ions accelerates the rate of corrosion of the metal by changing redox potentials of iron. Besides, Cl^- favors the formation of relatively large amounts of akaganeite (β-FeOOH) [10-13]. This oxide does not convert into goethite, which is one of the main components of the protective oxide layer of weathering steel and, besides, the one that exerts the protection [14]. In addition, magnesium salts are also concentrated in marine environments. It has been checked that a high concentration of Mg in the rust layer has a great influence on the corrosion behavior of weathering steel, especially on the later stage of the corrosion process, giving rise to the formation of β-FeOOH, magnetite (Fe_3O_4) and lepidocrocite (γ-FeOOH), which are the most active phases of the protective layer of weathering steel and did not give any protection to the metal. Moreover, complex corrosion phases can also be formed such as magnesioferrite ($MgFe_2O_4$) and iowaite ($Mg_4Fe(OH)_8OCl{\cdot}4H_2O$) [15].

Finally, silicate particles are sometimes highly concentrated in most of the atmospheres. The presence of any kind of silicate matter has a huge effect in the evolution of the protective rust layer of weathering steel. This patina is composed by different iron oxyhydroxides that change with the exposure time. In the first stages of the exposition the main iron phase present in the steel surface is lepidocrocite that is an active phase and does not exert any kind of protection. Over the years, this lepidocrocite is transformed into goethite that is the most stable iron compound and is the responsible for the atmospheric corrosion protection since it acts as a barrier against the corrosion phenomenon [16-18]. The presence of silicates inhibits and retards the transformation of lepidocrocite into goethite, and in consequence, the passivation of the rust layer. Therefore, the protective ability is reduced [16-18].

Taking into account the effects that the presence of some particles can have in the development and the conservation of weathering steel structures, it is crucial the study of the conservation state of artworks or other structures made of this material and the assessment of the impacts that the deposition of particles could be having in the material. The more suitable analytical techniques that can be used for the characterization of deposited particles are the so-called non-destructive ones, since sampling a great amount of material in artworks or buildings can affect to the surface homogeneity and therefore, to the visual appearance. Among these kinds of techniques there are several that can be used for the off-line study of particles, no matter if they are sampled by passive methods of if they are deposited on a surface. For instance, infrared spectroscopy [19, 20] or Raman spectroscopy [20] but most of the articles

published in this field have employed SEM or TEM sometimes coupled to EDS o EDX analyzers due to their high resolution [21-23]. However, from the characterization point of view using TEM or SEM coupled to EDS only elemental information can be extracted. In addition, in those cases where atmospheric particles deposited on a surface want to be analyzed with molecular techniques (Raman or Infrared spectroscopy) there are some drawbacks related to the particle size and the background, i. e. the studied surface. Even though the analysis of the particles are performed using microscopy, if the particle size is too small and taking into account that the background gives, normally, a huge signal, Raman or Infrared signals belonging to the particles cannot be detected. To avoid these problems, the use of the so-called SCA emerging technique (Structural and Chemical Analyzer) that couples Raman micro-spectroscopy and SEM-EDS measurements in the same spot area, seems to be an adequate alternative. By this technique, really specific elemental and molecular analysis of particles can be performed, such as those performed on metallic dust particles from abandoned mine areas [24] or from black slag materials [25].

In this work different weathering steel structures exposed in an urban-industrial atmosphere are studied. These structures present some flaking processes and some discoloration areas in their surfaces, which is a worrying problem. Through some previous works it was intuited that some of these problems could be generated by deposited particles [26-28]. In this way and in order to deepen in this problem, in the present paper a deep study of the characterization of different atmospheric particles and an assessment of their possible consequences in the steel surface has been carried out.

2. MATERIALS AND METHODS

Structures and location

In this study five steel structures were analyzed. All of them were made in weathering steel with little variations in the elemental composition or in the manufacture used in the fabrication. The main characteristics are summarized in Table 1. They are exposed to the same urban-industrial atmosphere of Bilbao city, Northern Spain, subjected to several pollution or/and particle sources such as traffic, urban works, marine airborne, etc. Bilbao is the largest city of the Basque Country and it is located around 14 kilometers south of the Golf of Biscay, where the estuary of Bilbao is formed. The entire city is crossed by the Nerbioi-Ibaizabal

estuary, which is subjected to tidal effects. Its main urban core is surrounded by two small mountain ranges and the surrounding is formed by limestone and sandstones mainly [27].

The estuary is the most industrialized area in the Northern Spain since the 19th century. For more than 100 years a very important economic and industrial activity has been developing in the estuary banks. In the last decades, the environmental problems started to be a social worry and therefore some human activities were stop. Nowadays, in Bilbao Metropolitan area the industrial pressure is still present, with steel industry, harbor activities and chemical plants. However, the high traffic has become the main pollution source [29, 30]. Actually, in 2007 the average value in air for CO_3^{2-}, SO_4^{2-}, NO^{3-}, Ca and SiO_2 were 8.5, 2.5, 2.5, 5.6, 6.2 $\mu g/m^3$ respectively [32]. In addition, the atmosphere of Bilbao is of an acid nature and Bilbao's climate is characterized by a high number of rainy days and a high annual rainfall rate. In fact, the annual precipitation is 1170 mm and they are 3000 hours per year of wetness. Due to these humidity conditions, together with the high concentration of industrial acid gases, Bilbao city is considered a high corrosive atmosphere, inside the C4 corrosion category by the ISO 9223 [31]. All these factors make the particle deposition and the material degradation considerable.

In this kind of studies it is crucial to know the direction of the winds. In this case, the predominant winds in Bilbao city have west component due to topographic conditions covering its influence from March to August, having a maximum in June. During autumn and winter the frequencies of the eastern components are predominant [32].

Equipments and methods

For this work the combination of SEM-EDS (Scanning Electron Microscopy-Energy Dispersive Spectroscopy) and SCA (Structural and Chemical Analyser) device were used. This SCA interface allows the user to perform Raman spectroscopy simultaneously with Secondary Electron (SE) imaging inside the SEM, on the spot areas selected previously because the laser light and Raman signal are both transmitted between the Raman spectrometer and the SCA via 2 meters fiber optic cables up to the SEM vacuum chamber (Figure 1).

In this way, first, it is possible to perform a scanning chemical image of a micro area of the sample surface using SEM. Then it is possible to analyse that area identifying the present/absence elements using EDS, and finally, by SCA device it is possible to focus the laser beam on the point of interest to get Raman spectra. Therefore, this SEM-EDS/SCA device

allows to get elemental and molecular information of the same point. This approach resulted very useful for the identification of deposited particles and degradation compounds because the surface of the steel is very homogeneous from the elemental point of view and all the exogenous compounds were easily discerned from the background. Besides, by using SEM-EDS, the deposition rate of the detected compounds could be ascertained by the observation of EDS distribution maps, where it can be seen in a SEM image how many microns of the steel surface are covered by exogenous particles.

Weathering steel micro-samples were deposited on the surface of a special aluminium pin and glued to the surface by using a carbon adhesive tape. As the samples may contain carbon compounds, they were not covered with graphite or gold to avoid interferences. The experimental platform has three units. On the one hand, an EVO 40 Scanning Electron Microscope (Carl Zeiss NTS GmbH, Germany) coupled to an X-Max Energy-Dispersive X-Ray spectroscopy equipment (Oxford Instruments, UK) was used for electron image acquisitions and elemental composition determinations. SEM images were acquired at high vacuum employing an acceleration voltage of 20 KV. Magnifications up to 10000x were reached using a SE detector. EDS (Oxford Instruments, UK), was used for elemental mapping, and the analyses were performed using an 8.5mm working distance, a 35° take-off angle and an acceleration voltage of 20 KV. For the SEM-EDS data collection INCA suite 4.13 (Microanalysis Suite, UK) was used. This software allowed to perform chemical maps of all present elements in the scanning image simultaneously. The plots appear in black and white, where the former represents the absence of an element and the latter the presence of it. Besides, there is the possibility to perform false color images of the analyzed surface where the energies of each element are represent in different colors over the SEM image for a better visualization of the chemical maps.

The third unit is the SCA interface (Renishaw, UK), that uses in-SEM retractable collection optic to introduce the laser light and focus it into the sample as well as to collect the Raman signal through the in-Via micro-Raman spectrometer. This Raman micro-spectrometer has a Peltier-cooled (-70ºC) detector. The spectrometer is provided by a 514 and 785 nm laser. The power applied was set at the source at a maximum of 50 mW while on the sample was always less than 20 mW. The spectral resolution is around 1 cm^{-1}. The software used for the data collection is the Renishaw Wire 3.2. In order to avoid excessive noise in the spectra, the equipment is installed in an antivibratory table and in a temperature controlled room. In spite of this, with SCA device, the collected spectra are usually noisy and, therefore, very long measures (up to 40 seconds and 40 accumulations) are needed to obtain a good signal to noise ratio. For

conventional SEM-EDS analysis, the retraction mechanism of the SCA was used to quickly move the optic away to a 'standby' position. This operation mode was used to set the positions of the trace elements in order to better focus with the SCA interface.

The calibration of the Raman spectrometers was performed every day by using a silicon slice and its band at 520.5 cm^{-1}. For spectral analysis and treatment in all cases the Omnic software by Thermo Nicolet (USA) was used. Raman spectral interpretation was done by comparison with pure standard compounds contained in the spectral databases e-VISART and e-VISARCH [33, 34] and bibliography (see below).

This method is non-destructive; however, samples must be collected since the analyses must be performed in the laboratory. For that reason, in this case micro steel samples were taken carefully from the structure surfaces using a scalpel. Some parts of the steel surfaces were detaching, thus, in those cases, these samples were collected there in order to alter as less as possible the surface.

Some destructive analyses were performed in some cases when SCA technology was not enough to define a mineral phase. Following this aim, a soluble salt extraction and further quantification was carried out. The extraction was done using an adaptation of the Society of Protective Coatings (SSPC)-Guide 15 for "Retrieval and Analysis of Soluble Salts on Steel and Other Nonporous Substrates" [26, 35], and the quantification was carried out by using a Dionex ICS 2500 ionic chromatograph with a suppressed conductivity detector ED50 for the anions and cations and an Elan 9000 ICP-MS (PerkinElmer) for the metals [26].

3. RESULTS AND DISCUSSION

By means of SEM analyses and performing a scanning of the surface, several structures corresponding to the original compounds of the protective layer were distinguished. Lepidocrocite and goethite could be differentiated in these samples because of its morphology since the former has a "grass" appearance while the latter has "cotton ball" morphology [36]. These observations were corroborated by SCA (Figure 2). Through these analyses and observations it was possible to perform some initial conclusions about the conservation state of the structure considering the α/γ * *ratio* [37]. This index is used in steels to assess the evolution of the corrosion calculating the ratio between the most passive phase (goethite) and the most active phases (lepidocrocite and magnetite), and it can be seen how the protective rust layer is being developed [37]. In the analysed samples, a massive presence of lepidocrocite was

observed in structure 1 and 4 which indicated an anomalous evolution of the protective layer in these cases. However, in the other structures a higher presence of goethite was detected, which represents a better evolution of the protective layer, and therefore higher protection. Apart from the iron oxides and oxyhydroxides, chromite ($FeCr_2O_4$) was also detected through its main Raman band at 670 cm^{-1}. This compound is a sign of how the iron and other alloy elements react among each other.

In addition, SCA was used to analyze the particulate matter deposited over the steel surface and the degradation products generated as a consequence of the particles´ presence.

Before starting with the Raman (SCA) particles analyses, collected steel samples were analyzed in the laboratory under an optical microscope and a high deposition rate of particles which covered, in some cases, the entire steel surface was detected (Figure 3). In this figure the difference between the exposed face and the reverse of a sample from Structure 1 can be seen. The exposed side is completely covered by particulate matter while the reverse has almost no depositions.

The element distribution maps obtained by means of EDS and SEM images (see Figure 4 a, b and d) show the high deposition rates of calcium that are suffering the studied steel surfaces. By SCA, it was observed that the most identified particle deposited over all steel samples was calcite ($CaCO_3$), not rare since Bilbao city is located in a calcareous territory [27].

Raman (SCA) analyses carried out on weathering steel surfaces showed the presence of many calcite particles ($CaCO_3$, main Raman band at 1085 cm^{-1}) and high magnesium calcite particles (HMC, main band at 1090 cm^{-1}) [25, 38, 39]. These particles were detected mainly in Structure 1, 4 and 5 and in the case of 1 and 5, especially in the south orientation which were exposed to building works.

Together with calcite, the most deposited particles on the steel samples were silicate particles, especially in Structure 1, 4 and 5. Figure 5 shows the SEM-EDS mapping done over the surface of a chip from Structure 1. In Figure 5b a false color map of the same SEM image is represented. In that image, in yellow, the EDS energies of the silica are represented and in orange the energies of the aluminium, whereas in the background, in black and blue, the energies due to the presence of iron are represented. In Figure 5 c-h, the EDS distribution maps of each element are represented. By means of these distribution maps the composition of the silicates could be ascertained. For instance, magnesium and potassium aluminosilicates could be present in the steel surface (see Figure 5) since these elements were concentrated in the same

point. By SCA (Figure 5i), quartz (SiO_2) was identified. In addition, EDS spectrum (Figure 5j) confirmed the presence of potassium and magnesium aluminosilicates.

The size of the silicate particles can vary from 19 μm to 1 μm in the studied steel samples. Moreover, by means of the SEM images the deposition rate of the particles can be assessed. In the case of silicates, as it is shown in Figure 5, the deposition rate over the structure surface is very high. According to literature, this high presence of silicates in the protective layer of weathering steel could be inhibiting the transformation of lepidocrocite into goethite, [40] and in consequence, the passivation of the rust layer in some of the studied structures. This could be a reason that explains the high occurrence of lepidocrocite in some steel surfaces (Structure 1 and 4). This fact has further effects since if the protective rust layer is not well formed and if the goethite is not present in the surface, the protective ability of this layer would be reduced.

In contrast to Structure 1, 4 and 5, Structure 2 shows the lower presence of silicates. This could be due to the fact that this structure is located between two skyscrapers that could unshield the steel structure from the particle deposition. However, by means of SEM-EDS, the deposition rate of marine airborne could be seen, and as it was expected, this structure was the most affected one by marine effect since it is located in the bank of the estuary and exposed to the marine airborne. In the other studied structures chloride was also detected but not in the same extent as in Structure 2 (Supplementary material 1).

Some sulphates were detected by means of SCA. First, some translucent crystals were observed under a 50x optical microscope (Figure 6b) in the steel surface. These crystals were identified as gypsum (Raman main band at 1006 cm^{-1}) by means of Raman (SCA) spectroscopy and they appeared (see in Figure 6f) usually near magnetite crystals (grey areas of Figure 6b) in Structure 4 above all and especially in the south orientation of the structure, which is the one faced to the road traffic. The presence of this salt in the steel surface supposes the presence of other hydration form of calcium sulphate due to temperature changes. The transformation of one in another could induce a flaking process due to the physic stress generated by the volume differences among them (bassanite, gypsum and anhydrite) [26]. SEM-EDS resulted also very helpful in the study of the deposition rate of these particles (Figure 6a, e).

Some other suphates were also identified using SCA. This is the case of the Raman band at 1021 cm^{-1} that could belong to a manganese sulphate called szmikite ($MnSO_4 \cdot H_2O$, Figure 7). The obtained Raman spectra were very noisy, however, the elements' maps (Figure 7

c and d) and some previous data obtained in the laboratory (see below) by means of ionic chromatography, which confirmed the presence of soluble manganese sulphates on the steel surface, allowed us to confirm the presence of szmikite.

As the band for the szmikite was not very clear and the ratio signal-to-noise ratio was quite low, further analyses (soluble salt quantification) were carried out in order to confirm the presence of this mineral phase in the studied weathering steel surface. It must be said that this was the only case for which further analyses were needed, since, as it has been seen all along the present work, SCA technology was enough for the determination of the minerals present in the surface.

Quantitative analyses performed with Structure 5 revealed that there was a high concentration of soluble manganese (Table 2) present in the surfaces. The possible origin of this compound could be the SO_x since in the correlation analyses the sulphate and manganese were positively correlated. In addition, in order to define how the szmikite is formed on the steel surface, a thermodynamic chemical simulation was done using the MEDUSA software [41]. For this purpose and in order to define the variables (pH and redox) for the modeling, dripping water coming from the structures were collected and measured in-situ. Redox potential varied from 89 to 91 mV, thus, it was decided to set it at 90 mV. The measured pH value was 6. Besides, the temperature used for the simulations was 25ºC in all cases. Finally, the most relevant pollutant gases present in the environment of Bilbao (SO_2 and CO_2) were introduced based in the data from air quality stations placed near the structures [42].

In Supplementary Information 2 the thermodynamic modeling of the szmikite is showed. There, it can be seen how in the Bilbao atmosphere conditions the szmikite is formed from metallic manganese by SO_2 attack in the weathering steel. The manganese sulphate is very soluble (59.6 g/100 g at 70ºC) and, therefore, it can be lixiviated by the rainfall with the consequent material lost. In the figure it can be seen also that at the established conditions and at low concentration of SO_2, manganese carbonate is formed. However, this compound has not been identified in the steel surface.

In previous studies it was confirmed that iron and nickel (which is an alloy element) are attacked by atmospheric SO_2 giving rise to their respective soluble sulphates, rozenite ($FeSO_4 \cdot 7H_2O$) and retgersite ($NiSO_4 \cdot 6H_2O$), following a similar process to the manganese [26]. With this study, it has been confirmed that the manganese, that is another alloy element in weathering steel composition, is also attacked by SO_2 and then lixiviated.

Other particles coming from the traffic and the industry were identified in the studied weathering steel surfaces. In the SEM image shown in Figure 8a, a titanium particle can be seen represented in green in the false color image (EDS spectrum seen in Figure 8b). Moreover, by means of common Raman spectroscopy anatasa (TiO_2) (impossible to detect by SCA perhaps due to the little size of anatasa aciculums) was identified by its main Raman band at 147 cm^{-1} (Figure 8c). Besides, mineral carbon particles were deposited over the structures´ surfaces. In Figure 8d another SEM image of Structure 1 surface is shown. On the top, the central figure is an EDS color mapping of a SEM image in which the carbon energies are represented in orange, silicon energies in yellow, and the background, composed mainly by iron and oxygen, in blue and red. Over the background, apart from silica compounds (quartz, silicates of aluminum and magnesium in green and yellow), carbon (charcoal, orange) can be seen, as it can be seen in Figure 8e. Charcoal was also characterized by means of laboratory SCA coupled to SEM-EDS (Figure 8f).

4. CONCLUSIONS

As it has been demonstrated SCA technology is a very good tool for the identification and assessment of the role of different atmospheric particles in the weathering steel surface due to the relative homogeneous composition of the steel, which allow to discern perfectly any exogenous material different from the background. It must be said also that sometimes, depending on the conditions of the surface (fluorescence, presence of dust or organic matter, dirt, etc.) Raman spectra could be very noisy and of bad quality making the identification of peaks and the assignment of those peaks almost impossible. However, the knowledge of the sample and the supplementary information provided by the chemical maps of the elements (SEM-EDS) make easier this task.

Regarding weathering steel, these structures, which are exposed to urban industrial atmosphere, are really affected by atmospheric deposition. There has also seen that the marine airborne is not as harmful as the presence of silicates for the evolution of the material since Structure 2 is the most affected structure by the marine airborne and it is not in so bad conservation state as Structure 1, 4 and 5, which are really affected by silicate deposition. Thus, it can be said that the effect of silicates is more severe for the weathering steel than that of sodium chloride.

Finally, it has been seen also that the acid gases, mostly SO_2, attack the alloy elements of the weathering steel. In recent studies it was seen this fact in the lixiviation process of Ni and Fe, and in the present work this issue has been observed also in the lixiviation process of Mn.

ACKNOWLEGEDMENTS

J. Aramendia and L. Gomez-Nubla are grateful to the University of the Basque Country (UPVEHU) for their post-doctoral and pre-doctoral grants. We would like to thank Bilbao Guggenheim Museum, BBVA bank and Bilbao City Council for all the support during the analysis of the structures. This work has been funded by the Spanish Ministry of Economy and Competitiveness (MINECO) through the project DISILICA-1930 (ref. BIA2014-59124). Authors thank Raman-LASPEA Laboratory from the SGIker (UPV/EHU, MICINN, GV/EJ, ERDF and ESF) of the University of the Basque Country and Alfredo Sarmiento for their collaboration in the analyses.

REFERENCES

[1] D. Farb, M. A. Stockwell, Modern steel construction, American Institute of Steel Construction, New York, 1975.

[2] M. Mostafavi, D. Leatherbarrow, On Weathering: The Life of Buildings in Time, Massachusetts Institute of Technology, Massachusetts, 2005.

[3] C. Chiavari, E. Bernardi, C. Martini, F. Passarini, A. Motori, M. C. Bignozzi, Atmospheric corrosion of Cor-Ten steel with different surface finish: Accelerated ageing and metal release, Mater. Chem. Phys. 136 (2012) 477-486.

[4] S. Syed, Atmospheric corrosion of materials. Emirates J. Eng. Res. 11 (2005) 1-24.

[5] M. Maguregui, A. Sarmiento, I. Martinez-Arkarazo, M. Angulo, K. Castro, G. Arana, N. Etxebarria, J. M. Madariaga, Analytical diagnosis methodology to evaluate nitrate impact on historical building materials. Anal. Bioanal. Chem. 391 (2008) 1361-1370.

[6] C. Arroyabe, F. A. Lopez, M. Morcillo, The early atmospheric corrosion stages of carbon steel in acidic fogs. Corros. Sci. 37 (1995) 1751-1761.

[7] C. Arroyabe, M. Morcillo, The effect of nitrogen oxides in atmospheric corrosion of metals. Corros. Sci. 37 (1995) 293-305.

[8] L. Hao, S. Zhang, J. Dong, W. Ke, Evolution of corrosion of MnCuP weathering steel submitted to wet/dry cyclic tests in a simulated coastal atmosphere. Corros. Sci. 58 (2012) 175-180.

[9] L. Hao, S. Zhang, J. Dong, W. Ke, Evolution of atmospheric corrosion of MnCuP weathering steel in a simulated coastal-industrial atmosphere. Corros. Sci. 59 (2012) 270-276.

[10] R. E. Melchers, A new interpretation of the corrosion loss processes for weathering steels in marine atmospheres. Corros. Sci. 50 (2008) 3446-3454.

[11] Q.C. Zhang, J.S. Wu, J.J. Wang, W.L. Zheng, J. G. Ghen, A.B. Li, Corrosion behavior of weathering steel in marine atmosphere. Mater. Chem. Phys. 77 (2003) 603-608.

[12] J.K. Saha, Corrosion of Constructional Steels in Marine and Industrial Environment, Springer, Kolkata, 2013.

[13] T. Kamimura, S. Hara, H. Miyuki, M. Yamashita, H. Uchida, Composition and protective ability of rust layer formed on weathering steel exposed to various environments. Corrosi. Sci. 48 (2006) 2799-2812.

[14] D.C. Cook, Spectroscopic identification of protective and non-protective coatings on steel structures in marine environment. Corros. Sci. 47 (2005) 2550-2570.

[15] J. Wang, Z. Y. Wang, W. Ke, Corrosion behaviour of weathering steel in diluted Qinghai salt lake water in a laboratory accelerated test that involved cyclic wet/dry conditions. Mater. Chem. Phys. 124 (2010) 952-958.

[16] Y. Waseda, S. Suzuki, Characterization of corrosion products on steel surfaces, Springer, Sendai, 2005.

[17] D.A. Shifler, T. Tsuru, P.M. Natishan, Ito S., Corrosion in Marine and saltwater environments II. The Electrochemical Society, New Jersey, 2005.

[18] Y. Qian, C. Ma, D. Niu, J. Xu, M. Li, Influence of alloyed chromium on the atmospheric corrosion resistance of weathering steels. Corros. Sci. 74 (2013) 424-429.

[19] L. M. Russell, R. Bahadur, L. M. Hawkins, J. Allan, D. Baumgardner, P. Q. Quinn, T. S. Bates, Organic aerosol characterization by complementary measurements of chemical bonds and molecular fragments, Atmos. Environ. 43 (2009) 6100–6105.

[20] J. S. Gaffney, N. A. Marley, J. K. Smith, Characterization of Fine Mode Atmospheric Aerosols by Raman Microscopy and Diffuse Reflectance FTIR, J. Phys. Chem. A 2015, **DOI:** 10.1021/jp510361s.

[21] S. H. Lee, H. C. Allen, Analytical Measurements of Atmospheric Urban Aerosol, Anal. Chem. 84 (2011) 1196-1201.

[22] J. M. Conny, S. M. Collins, A. A. Herzing, Qualitative Multiplatform Microanalysis of Individual Heterogeneous Atmospheric Particles from High-Volume Air Samples, Anal. Chem. 86 (2014) 9709-9716.

[23] A. Laskin, J. P. Cowin, M. J. Iedema, Analysis of individual environmental particles using modern methods of electron microscopy and X-ray microanalysis, J. Electron. Spectrosc. 150 (2006) 260-274.

[24] N. Goienaga, A. Sarmiento, M. Olivares, J.A. Carrero, L.A. Fernandez, J. M. Madariaga, Emerging Application of a Structural and Chemical Analyzer for the Complete Characterization of Metal-Rich Particulate Matter, Anal. Chem. 85 (2013) 7173-7185.

[25] L. Gomez-Nubla, J. Aramendia, S. Fdez-Ortiz de Vallejuelo, K. Castro, J. M. Madariaga, From Portable to SCA Raman devices to characterize harmful compounds contained in used black slag produced in Electric Arc Furnace of steel industry. J. Raman Spectrosc. 44 (2013) 1163-1171.

[26] J. Aramendia, L. Gomez-Nubla, I. Arrizabalaga, N. Prieto-Taboada, K. Castro, J. M. Madariaga, Multianalytical approach to study the dissolution process of weathering steel: The role of urban pollution. Corros.Sci. 76 (2013) 154-162.

[27] J. Aramendia, L. Gomez-Nubla, K. Castro, I. Martinez-Arkarazo, D. Vega, A. Sanz López de Heredia, A. García Ibáñez de Opakua and J. M. Madariaga, Portable Raman study on the conservation state of four CorTen steel-based sculptures by Eduardo Chillida impacted by urban atmospheres. J. Raman Spectrosc. 43 (2012) 1111-1117.

[28] J. Aramendia, L. Gomez-Nubla, K. Castro and J. M. Madariaga. Spectroscopic speciation and Thermodynamic modeling to explain the degradation of weathering steel surfaces in SO_2 rich urban atmospheres. Microchem. J. 115 (2014) 138-145.

[29] I. Martínez-Arkarazo, M. Angulo, L. Bartolomé, N. Etxebarria, M. A. Olazabal, J. M. Madariaga. An integrated analytical approach to diagnose the conservation state of building materials of a palace house in the metropolitan Bilbao (Basque Country. North of Spain). Anal. Chim. Acta 584 (2007) 350-359.

[30] N. Prieto-Taboada, M. Maguregui, I. Martinez-Arkarazo, M. A. Olazabal, G. Arana, J. M. Madariaga. Spectroscopic evaluation of the environmental impact on black crusted modern mortars in urban–industrial areas. Anal. Bioanal. Chem. 399 (2011) 2949-2959.

[31] ISO 9223, Corrosion of Metals and Alloys – Classification of Corrosivity of Atmospheres, ISO, Geneva, 1990.

[32] M. Viedma, El régimen de vientos en la cornisa Cantábrica, Nimbus. 15-16 (2005) 203-222.

[33] K. Castro, M. Perez-Alonso, M. D. Rodriguez-Laso, L. A. Fernández, J. M. Madariaga, On-line FT-Raman and dispersive Raman spectra database of artists' materials (e-VISART database). Anal. Bioanal. Chem. 382 (2005) 248-258.

[34] M. Pérez-Alonso, K. Castro and J.M. Madariaga, Vibrational Spectroscopic Techniques for the analysis of artifacs with historical, artistic and archaeological value. Curr. Anal. Chem. 2 (2006) 89-100.

[35] Field methods for retrieval and analysis of soluble salts on steel and other nonporous substrates, SSPC Technology guide 15, Pittsburg, 2005.

[36] R. A. Antunes, I. Costa, D. L. A. de Faria. Characterization of corrosion products formed on steels in the first months of atmospheric exposure. Materia. 3 (2003) 403-408.

[37] J. Aramendia, L. Gomez-Nubla, L. Bellot-Gurlet, K. Castro, C. Paris, P. Colomban and J. M. Madariaga, Protective ability index measurement through Raman quantification imaging to diagnose the conservation state of weathering steel structures. J. Raman Spectroscop. 45 (2014) 1076-1084.

[38] W. D. Bischoff, S. K. Sharma, F. T. MacKenzie, Carbonate ion disorder in synthetic and biogenic magnesian calcites: a Raman spectral study. Am. Mineral. 70 (1985) 581-589.

[39] N. Arrieta, N. Goienaga, I. Martínez-Arkarazo, X. Murelaga, J.I. Baceta, A. Sarmiento, J.M. Madariaga, Beachrock formation in temperate coastlines: Examples in sand-gravel beaches adjacent to the Nerbioi-Ibaizabal Estuary (Bilbao, Bay of Biscay, North of Spain). Spectrochim. Acta A., 80 (2011) 55-65.

[40] U. Schwertmann, R.M. Taylor, The influence of silicate on the transformation of lepidocrocite to goethite. Clays Clay Miner. 20 (1972) 159-164.

[41] I. Puigdomenech, MEDUSA (Make Diagrams Using Sophisticated Algorithms), version 15; Department of Inorganic Chemistry, The Royal Institute of Technology: Stockholm, Sweden. http://www.kth.se/che/medusa (last accessed March 2015).

[42] Homepage of Basque Government (Air Quality Information), http://www.ingurumena.ejgv.euskadi.net , (last accessed March 2015).

Table 1. Main characteristics of the studied weathering steel structures.

Structure	Location and environmental aspects	History and manufacture	Maintenance
Structure 1	Faced to the Nerbioi-Ibaizabal estuary by the north orientation, to a traffic road by the east, to some works by the south and protected by the west.	Exposed outdoor since 2004 to the same environment. Produced in CorTen steel A (with less Cu than traditional) from forged steel and scrap.	Brushing of the rust and washing with pressured water.
Structure 2	Isozaki Towers. Exosed to the Nerbio-Ibaizabal estuary by the north. Direct impact of estuary but not by road traffic.	Exposed outdoor in 2003 in a rural environment and in 2006 in urban environment. Produced in rolled *weathering steel*.	Brushing of the rust and washing with pressure water (2003-2006). Nothing else till present.
Structure 3	Gran Vía (Circular square). Affected by dense road traffic.	Exposed outdoor since 1997 in the present site. Produced in Reco forged steel (Cu, Mb, Cr-Ni).	None at the present.
Structure 4	Abandoibarra. By the Nerbio-Ibaizabal estuary by the north and affect by road traffic by the south.	Exposed outdoor since 2003 in the actual site. Produced in CorTen steel A (with less Cu than traditional) with forged steel and scrap.	Periodical washing with pressure water.
Structure 5	Near the Nerbioi-Ibaizabal estuary and affected by road traffic by the southeast. And in a protected area by the northwest.	Exposed outdoor since 2008 in the current site.	Brushing of the rust and washing with pressured water.

Table 2. Water soluble salts composition determined by ion chromatography and ICP-MS in $mg \cdot kg^{-1}$ for Structure 5 samples. The quantification limits for all analytes were always lower than 2 ppm and the calculated relative standard deviation (RSD) lower than 15%.

	1NWI	**2NWI**	**3NWI**	**4SEI**	**5SEII**	**6NWII**	**7NWII**	**8NWII**	**9SEII**
Mn	**875**	**9.2**	**156**	**690**	**731**	**519**	**2100**	**1296**	**680**
Fe	90	<LOQ	<LOQ	26	4.2	22	39	10.3	10.6
Co	4.2	0.04	0.1	3.4	0.8	0.5	2.9	2.1	0.3
Ni	62	0.4	0.9	22	10.2	7.0	47	27	0.9
Cu	7.8	0.8	0.9	11.3	1.5	2.3	8.0	6.1	1.0
Zn	8.2	2.6	2.7	2.3	2.4	1.1	11.2	3.7	2.7
F^-	18	10.5	13.6	21	23	43	81	29	15
Cl^-	149	78	106	77	128	239	205	266	249
NO_3^-	<LOQ	51	18	35	50	64	44	33	<LOQ
SO_4^{2-}	63	19	34	47	123	267	327	173	50
K^+	107	90	49	134	133	229	523	171	94
Sr^{2+}	3.9	2.3	2.5	2.9	5.0	10.6	9.1	7.6	3.2
Na^+	194	144	200	226	447	1025	540	629	180
Mg^{2+}	59	21	68	162	174	306	864	319	67
Ca^{2+}	1116	689	840	715	1572	3790	2344	2001	1068

FIGURE CAPTIONS

Figure 1. SEM-EDS and SCA device's scheme.

Figure 2. SEM images of **a)** Structure 1 steel surface where it can be seen lepidocrocite with its "grass" appearance. **b)** Structure 2 steel surface with goethite in "cotton balls". Raman SCA spectra of **c)** Lepidocrocite and **d)** Goethite collected in the same point of SEM image by means of SCA.

Figure 3. a, b, c) Microphotograph of a steel sample at different magnifications. **d)** Microphotograph of the reverse of the steel sample.

Figure 4. a) SEM image of the weathering steel sample from the south orientation of Structure 5. **b)** False color image done over the SEM image where calcium is represented in green color, magnesium and silicon in orange and iron in blue. In the middle, EDS maps for **c)** iron, **d)** calcium and **e)** magnesium are represented. On the bottom, EDS spectra of the most abundant particles present on the surface are shown **f)** silicate and possible HMC and **g)** calcite.

Figure 5. a) SEM image of Structure 1 sample. **b)** False color image of the SEM picture. **c)** Iron distribution. **c)** Silica distribution. **e)** Aluminum distribution. **f)** Magnesium distribution. **g)** Potassium distribution. **h)** Oxygen distribution. **i)** Raman (SCA) spectrum of quartz and **j)** EDS spectrum of an aluminosilicate.

Figure 6. **a)** SEM-EDS image over Structure 4 sample took from the south face where multiple gyspsum particles are deposited. **b)** Microscopic image of gypsum and magnetite crystals. **c)** Iron distribution, **d)** calcium distribution and **e)** sulphur distribution. **f)** Raman (SCA) spectrum of a calcium sulphate particle, which is gypsum.

Figure 7. a) SEM image of Structure 5 surface. **b)** Raman spectrum collected in the scanning surface of southeast sample of Structure 5. Distribution maps of **c)** sulphur and **d)** manganese.

Figure 8. a) False color image of SEM image of a titanium particle deposited over Structure 2 surface (Titanium energies represented in green). b) EDS spectrum and c) Raman spectrum of the titanium particle at 147 cm^{-1} (L, lepidocrocite). d) False color image of SEM image of a charcoal particle deposited over Structure 1 surface. e) Carbon distribution and f) Raman spectrum of the charcoal.

Supplementary material 1. Chloride maps for: on the right Structure 1 and on the left Structure 2.

Supplementary material 2. Thermodynamic modeling of the szmikite formation over a steel surface.

Figure 1


EVO 40


RENISHAW

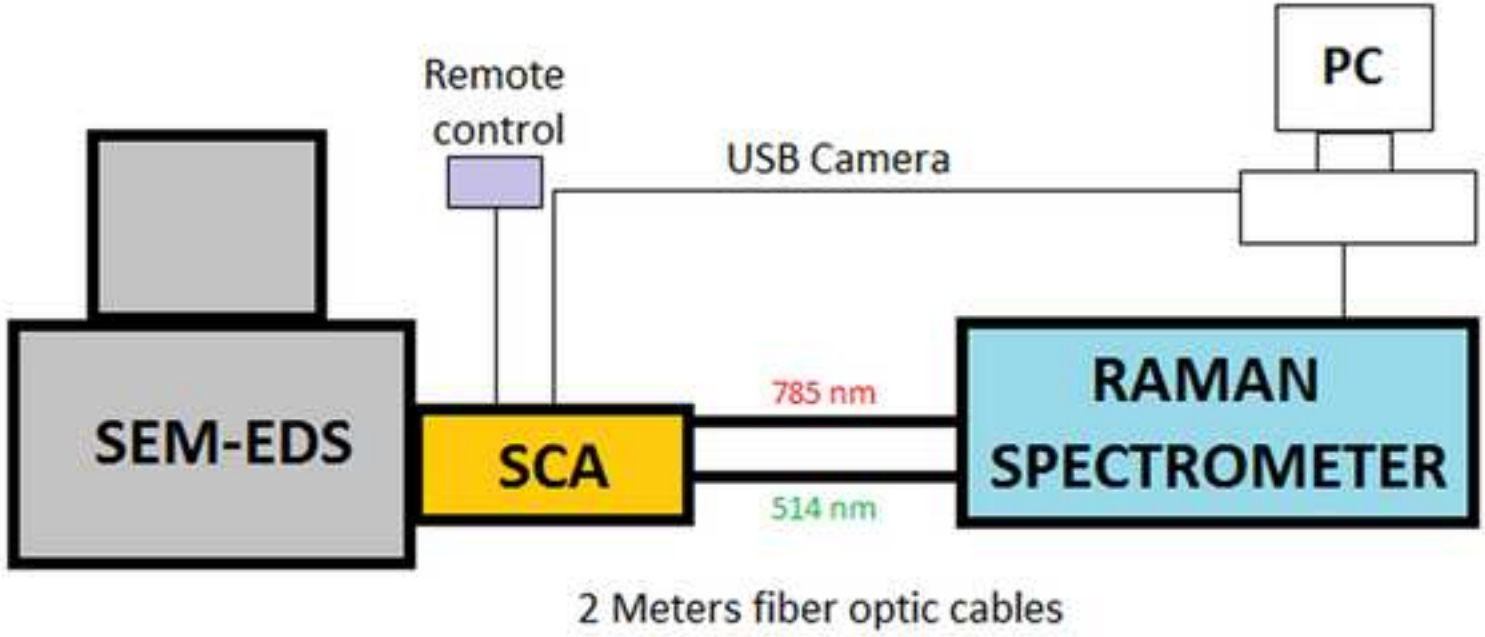
Remote control
PC
USB Camera
SEM-EDS
SCA
785 nm
514 nm
RAMAN SPECTROMETER
2 Meters fiber optic cables

Figure 2

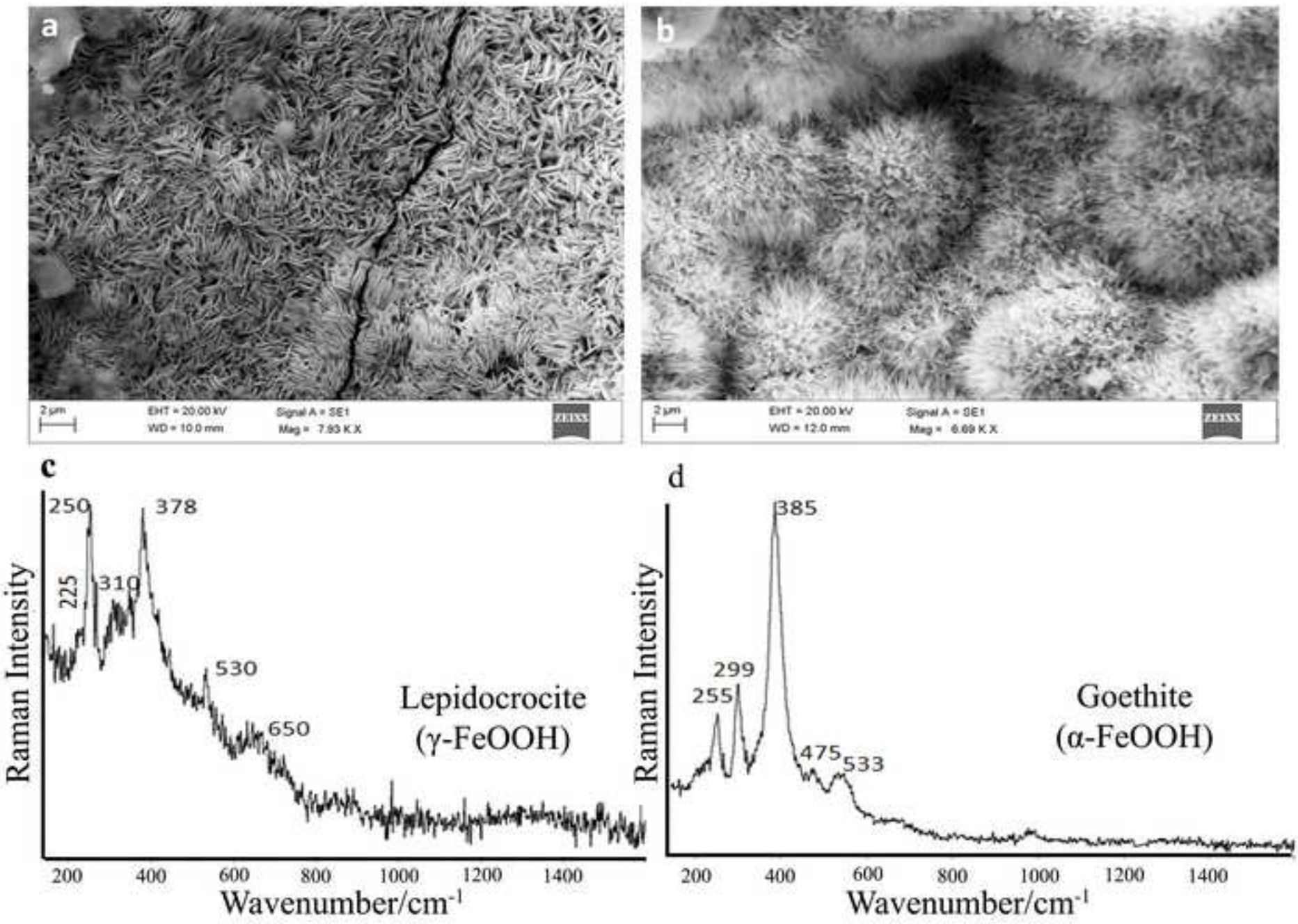
a
2 µm
EHT = 20.00 kV
WD = 10.0 mm
Signal A = SE1
Mag = 7.93 K X
b
2 µm
EHT = 20.00 kV
WD = 12.0 mm
Signal A = SE1
Mag = 6.69 K X
c
250
378
225
310
530
650
Lepidocrocite
(γ-FeOOH)
Raman Intensity
200
400
600
800
1000
1200
1400
Wavenumber/cm-1
d
385
299
255
475
533
Goethite
(α-FeOOH)
Raman Intensity
200
400
600
800
1000
1200
1400
Wavenumber/cm-1

Figure 3

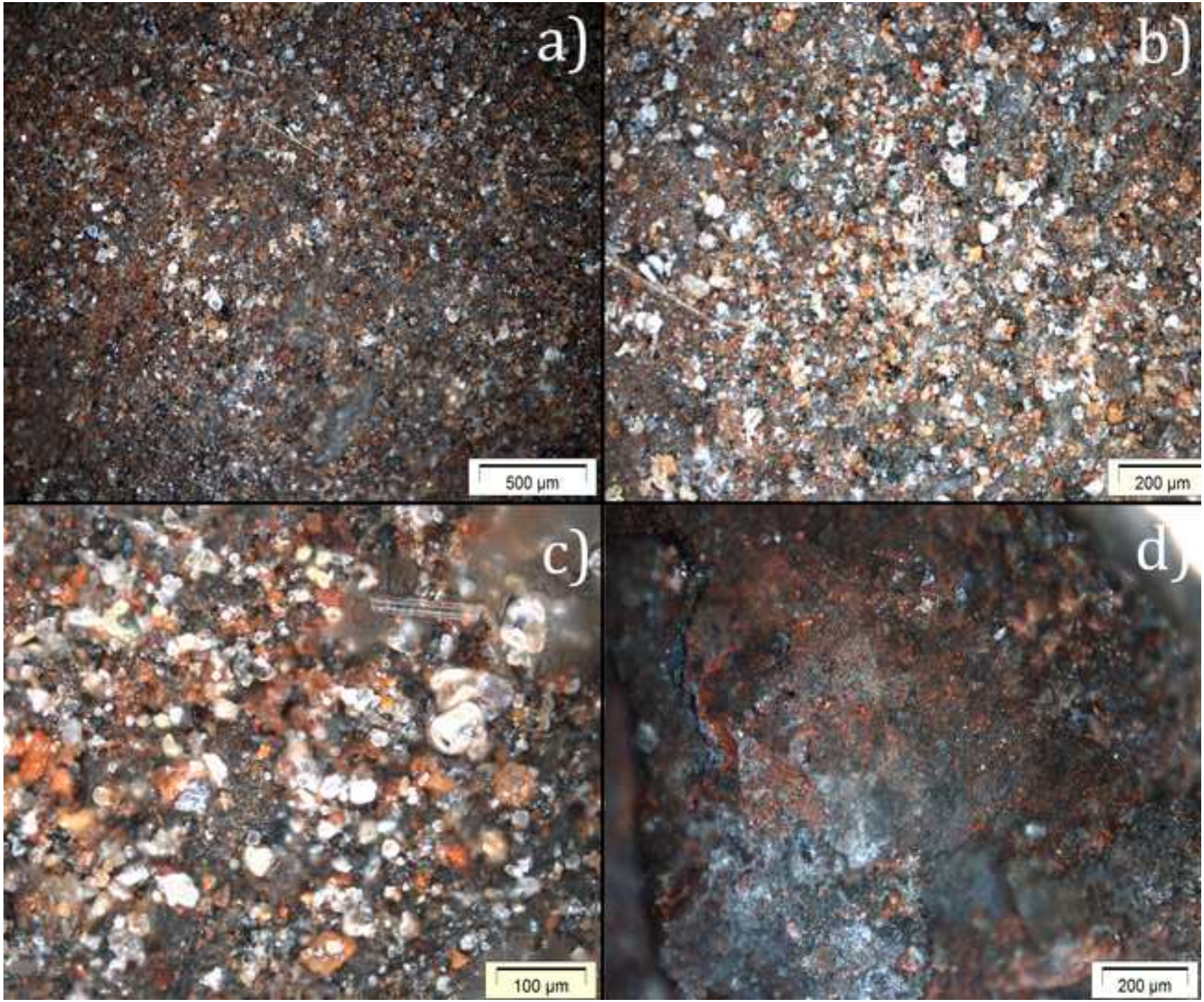

Figure 4

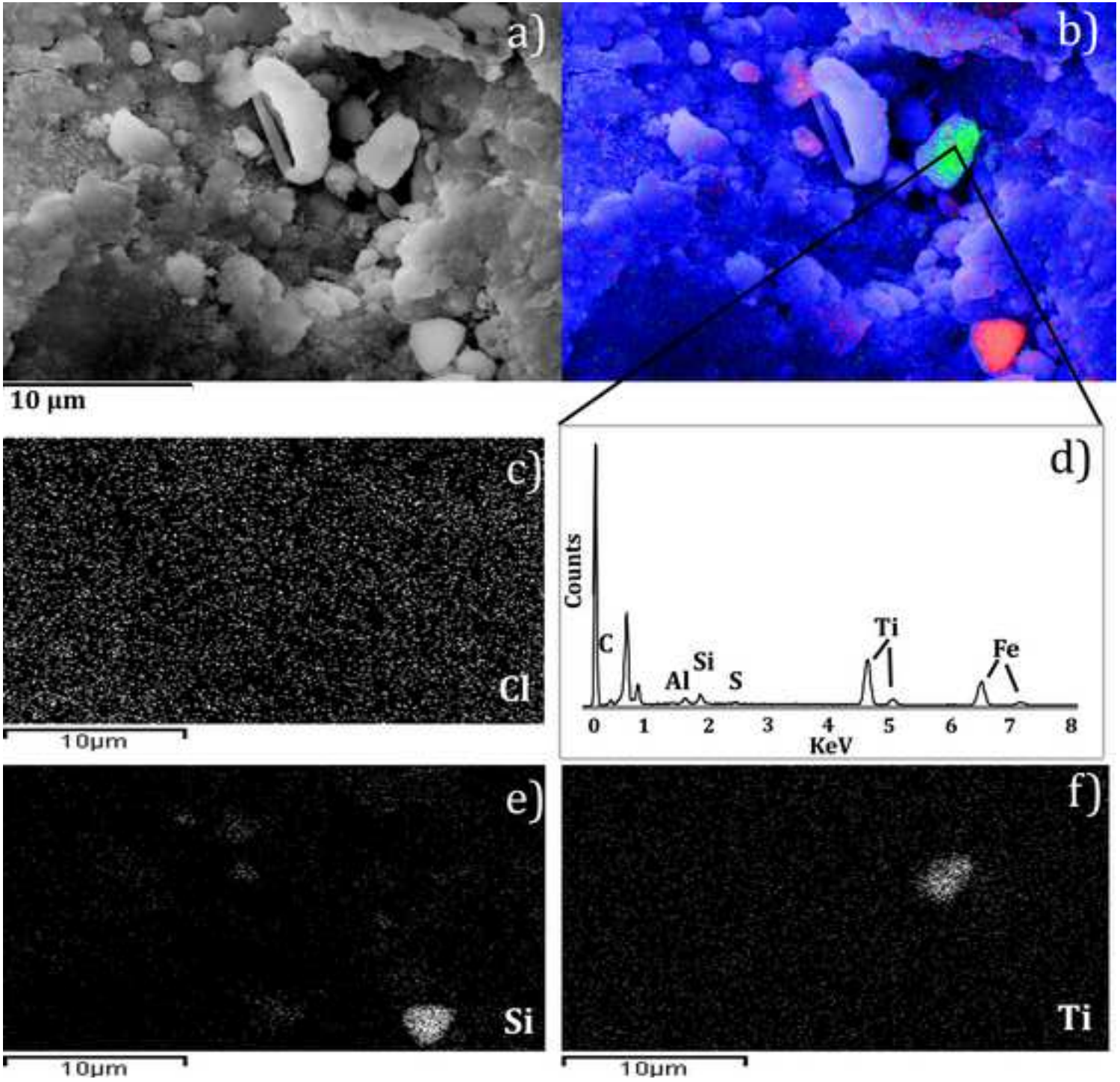
a)
b)
10 µm
c)
Cl
10µm
d)
Counts
C
Al
Si
S
Ti
Fe
0
1
2
3
4
5
6
7
8
KeV
e)
Si
10µm
f)
Ti
10µm

Figure 5

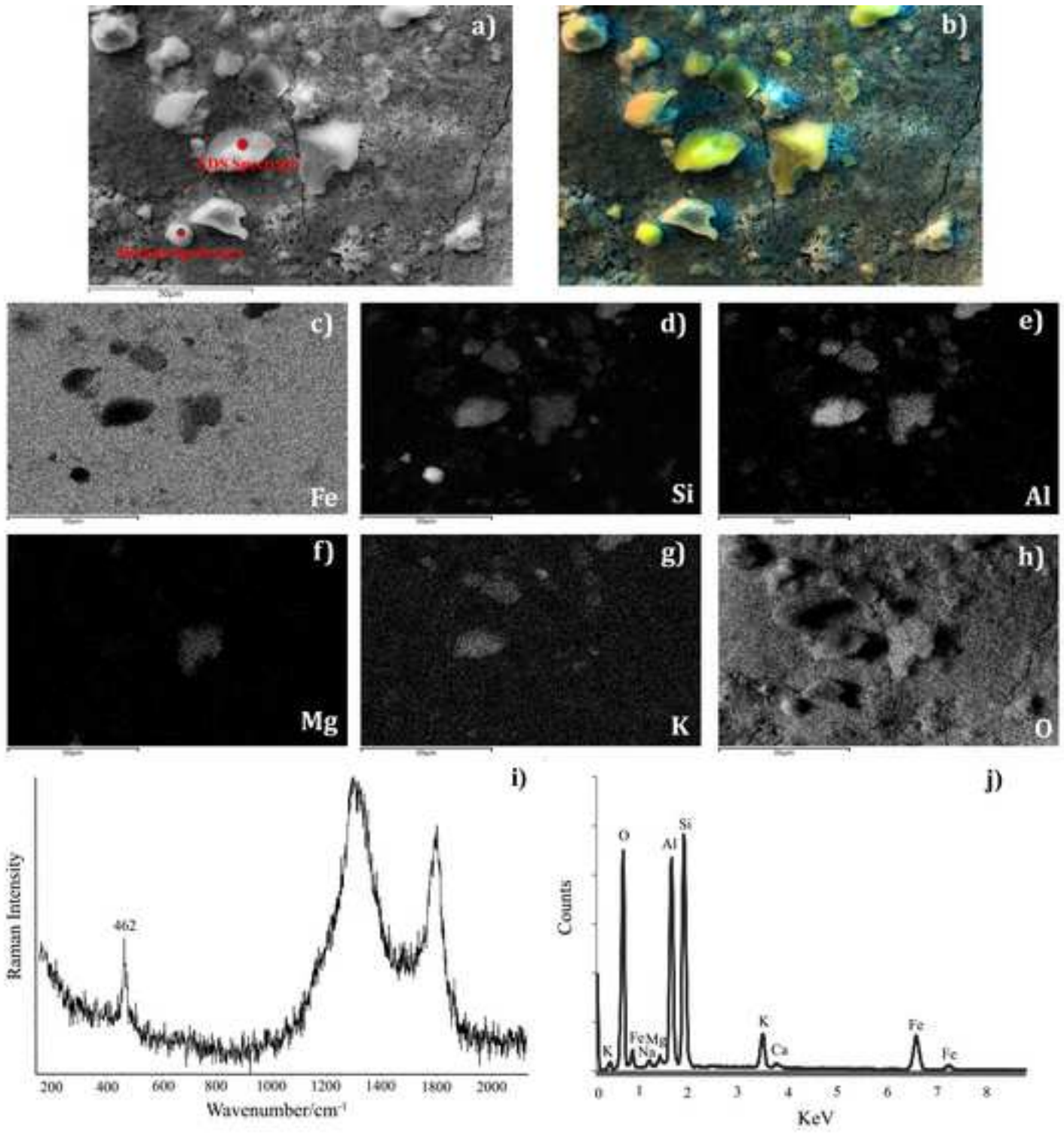
a)
b)
c)
Fe
d)
Si
e)
Al
f)
Mg
g)
K
h)
O
i)
Raman Intensity
462
200
400
600
800
1000
1200
1400
1800
2000
Wavenumber/cm⁻¹
j)
Counts
O
Al
Si
K
FeMg
Na
Ca
Fe
Fe
0
1
2
3
4
5
6
7
8
KeV

Figure 6

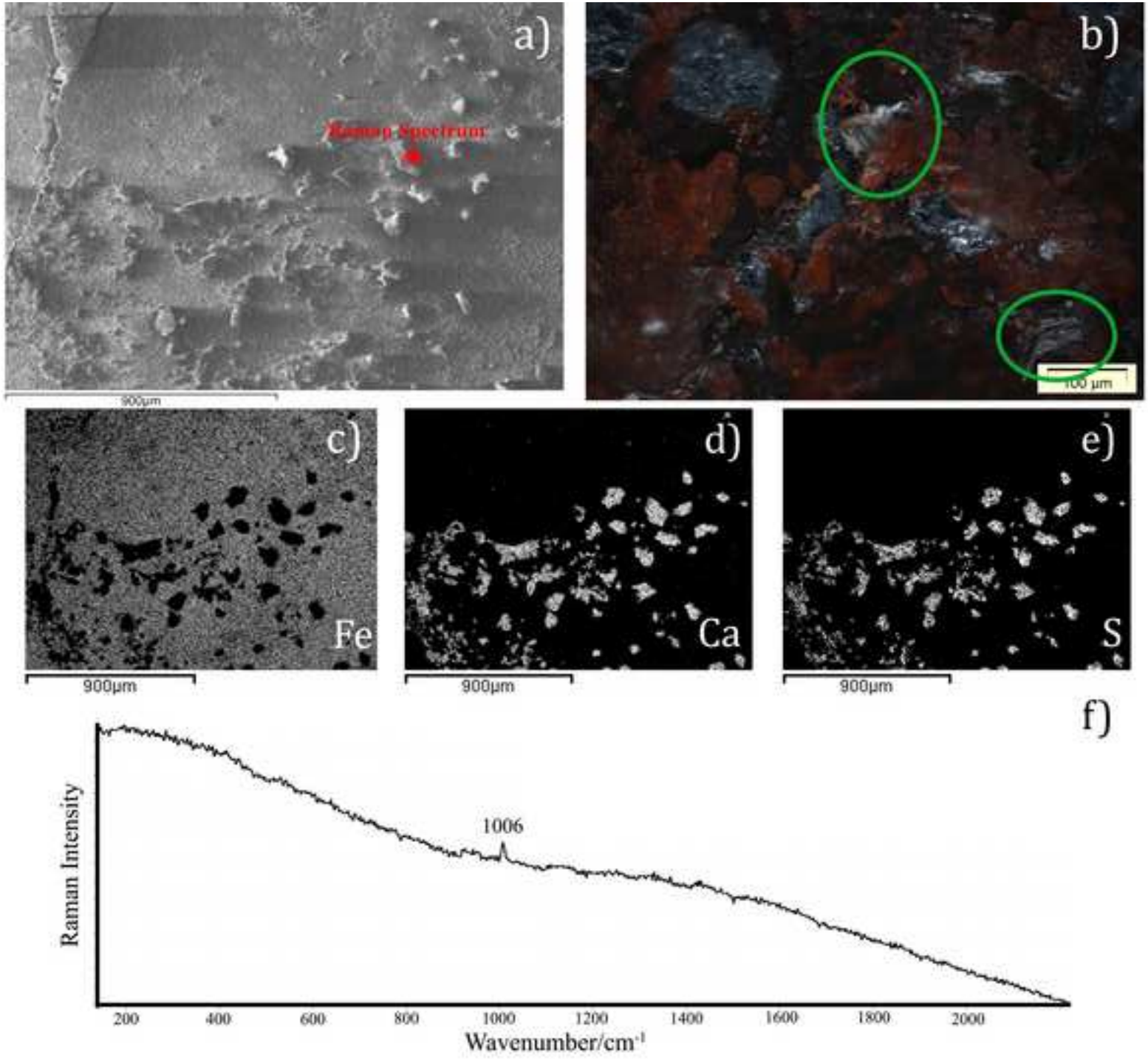
a)
Raman Spectrum
900μm
b)
100 μm
c)
Fe
900μm
d)
Ca
900μm
e)
S
900μm
f)
Raman Intensity
1006
200
400
600
800
1000
1200
1400
1600
1800
2000
Wavenumber/cm-1

Figure 7

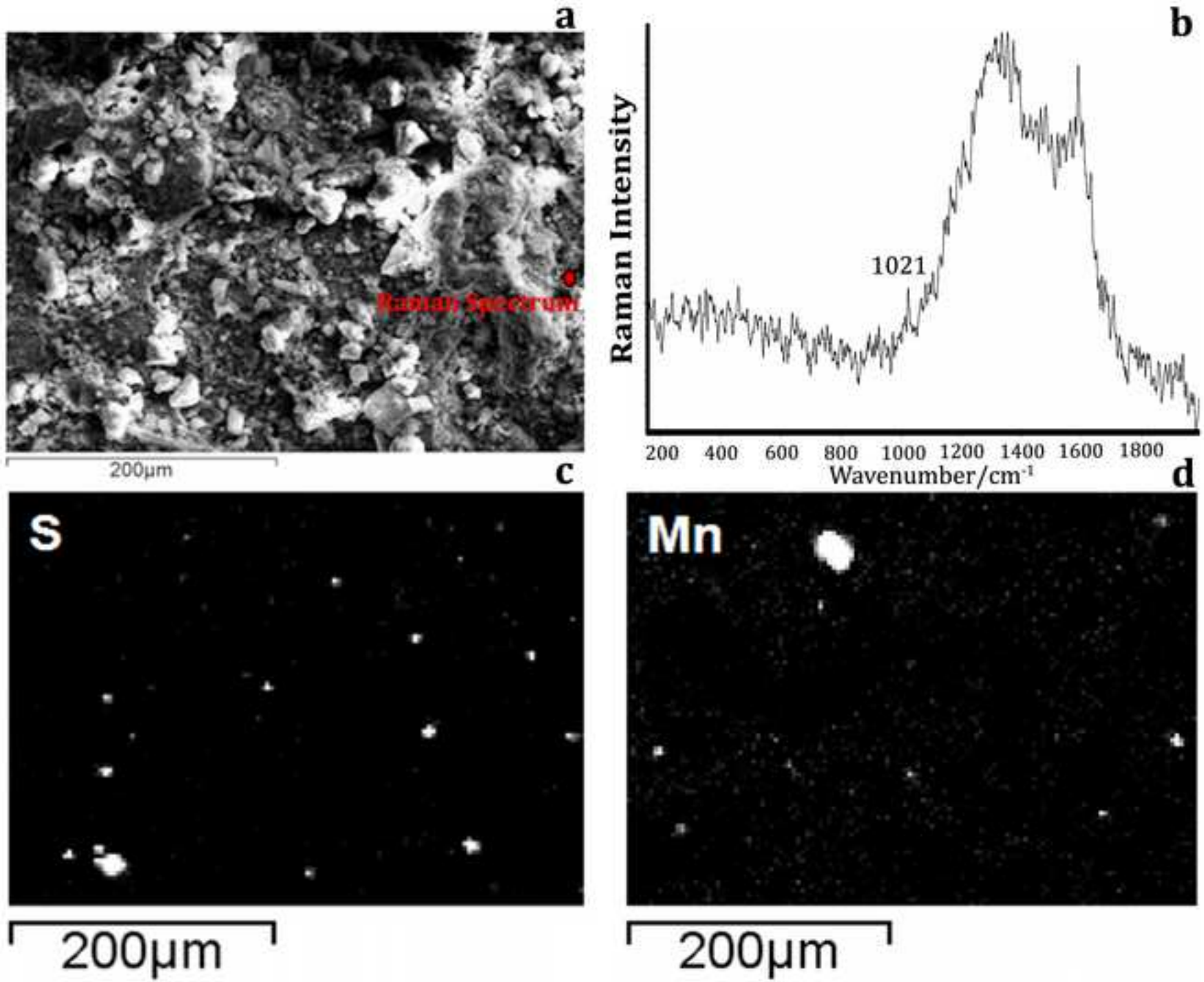
a
Raman Spectrum
200μm
b
Raman Intensity
1021
200 400 600 800 1000 1200 1400 1600 1800
Wavenumber/cm-1
c
S
200μm
d
Mn
200μm

Figure 8

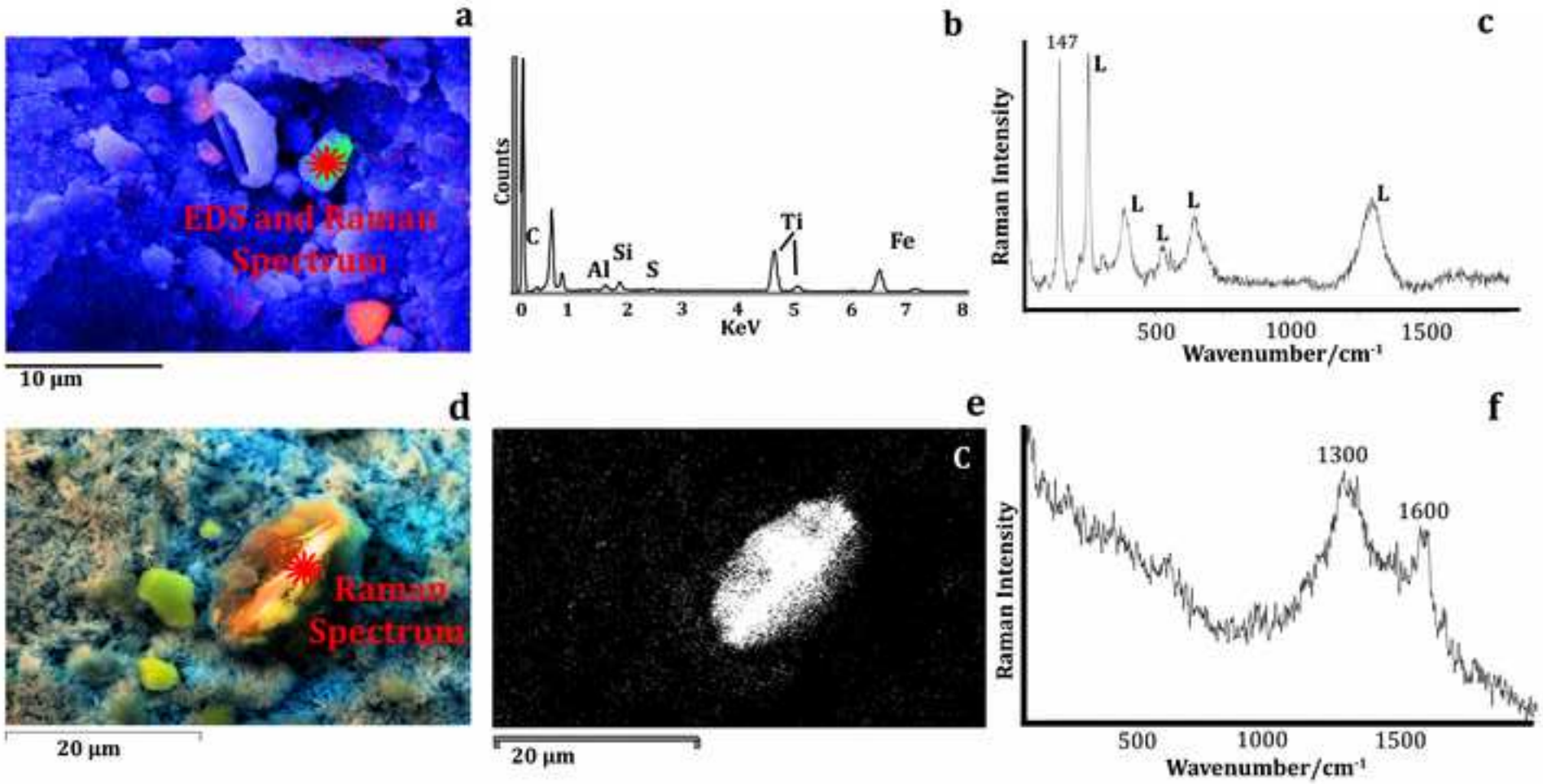
a
EDS and Raman Spectrum
10 µm
b
Counts
C
Al
Si
S
Ti
Fe
0 1 2 3 4 5 6 7 8
KeV
c
147
L
L
L
L
L
Raman Intensity
500 1000 1500
Wavenumber/cm⁻¹
d
Raman Spectrum
20 µm
e
C
20 µm
f
1300
1600
Raman Intensity
500 1000 1500
Wavenumber/cm⁻¹

Supplementary data

SUPPORTING INFORMATION FOR PUBLICATION

Supplementary material 1

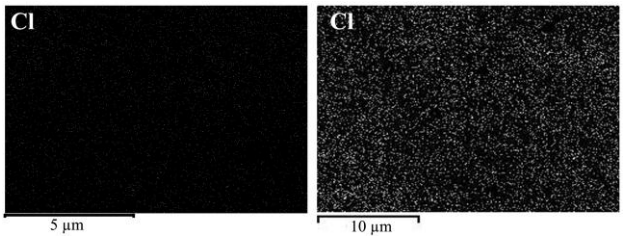

Supplementary material 2

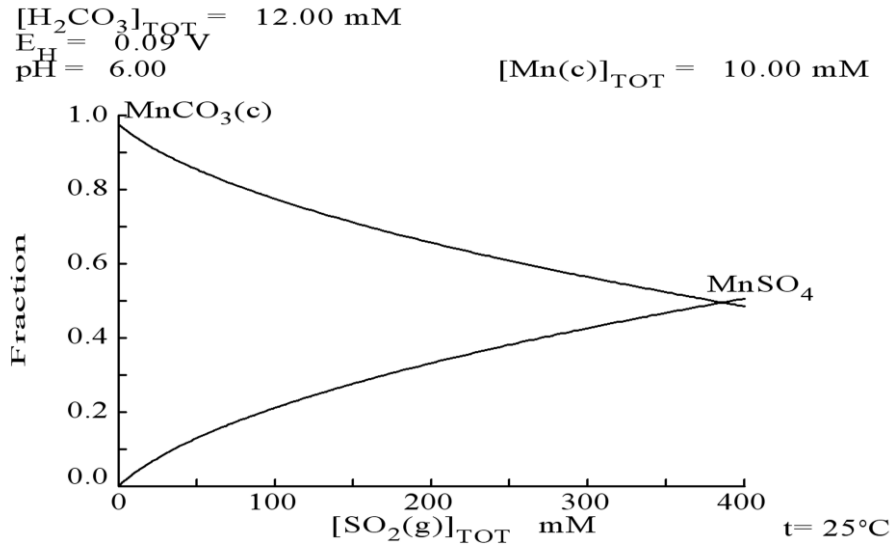

***Highlights (for review)**

- SCA novelty useful data for the study of weathering steel.
- Good results in the study of atmospheric particles deposited over steel.
- SEM-EDS useful for particles deposition ratio evaluation.
- Marine airborne is not as harmful as silicates for the evolution of the material.